Preparation of Binderless Activated Carbon Monolith from Pre-Carbonization Rubber Wood Sawdust by Controlling of Carbonization and Activation Condition

E. Taer[1,*], M. Deraman[2], R. Taslim[1] and Iwantono[1]

[1]*Department of Physics, University of Riau, 28293 Simpang Baru, Riau, Indonesia*
[2]*School of Applied Physics, Faculty of Science and Technology, Universiti Kebangsaan Malaysia, 43600 Bangi, Selangor, Malaysia*
**erman_taer@yahoo.com*

Abstract. Binderless activated carbon monolith (ACM) was prepared from pre-carbonized rubber wood sawdust (RWSD). The effect of the carbonization temperature (400, 500, 600, 700, 800 dan 900 °C) on porosity characteristic of the ACM have been studied. The optimum carbonization temperature for obtaining ACM with high surface area of 600 °C with CO_2 activation at 800 °C for one hour. At this condition, the surface area as high as 733 $m^2 g^{-1}$ could be successfully obtained. By improved the activation temperature at 900 °C for 2.5 h, it was found that the surface area of 860 $m^2 g^{-1}$. For this condition, the ACM exhibit the specific capacitance of 90 F g^{-1}. In addition the termogravimertic (TG)-differential termografimertic (DTG) and field emission scanning electron microscope (FESEM) measurement were also performed on the ACMs and the result has been studied. Finally, it was conclude that the high surface area of ACM from RWSD could be produced by proper selections of carbonization and activation condition.

Keywords: Activated carbon, Supercapacitor, Specific capacitance.
PACS: 81.05.U-, 82.47.Uv, 84.37.

INTRODUCTION

An activated carbon monolith (ACM) have recently attracted considerable attention because of their mechanical stabilities, electronic and thermal conductivities, and facilitated mass transport [1]. There characteristics make ACM to have a high potential for technological applications, such as in adsorption of harmful materials in liquid or gas phase, in catalyst support, and as carbon electrode for supercapacitor [2-4]. There are several different precursors and procedures to prepare acm that have been reported, e.g. the gel from resorcinol-formaldehyde and a catalyst by irradiation ultarsonic wave and then followed by carbonization and activation [5], the aerogels precursor in which micro and macroporosity is controlled by the choice of a block polymer [6], a mixture of styrene and divinylbenzene in dodecanol was filled into the void of silica monolith template and then carbonize and activation [7], the polymer (acrylonitrile, furfuryl accohol, pyrene and vinyl acetat) were templeted to zeolites and followed by carbonization [8], the mixture of mesophase and activating agent by mould conforming under pressing and followed by heated-treatment [9], the carbon powder from biomass precursor (olive stone) by using a proper binders [10]. The used of acm is rather limited at present due to high cost associated with the complicated preparation procedures.

In general, activated carbon from biomass precursors are produced in powder or granular forms. For fabricating ACM in monolithic form, a binder is requare to bind them together to form a requared shape. Attempt to produce ACM without using binding agent have been made using mesophase precursor [11]. Some study has been reported to produce the free binder ACM from biomass precursor, i.e. coffee endocarp [12], self adhesive carbon grain (SACG) from fibers of oil empty fruit bunch (EFB) [13]. Rubber wood sawdust (RWSD) have been used to produce SACG to prepare ACM for supercapacitor application [14,15]. In the present study, RWSD has also been used to produce ACM but the improvement of its porosity has been made by optimizing the carbonization temperature, activation temperature and holding time during activation based on one-step activation process. This optimization study has been reported elsewhere for carbon from coconut shell [16] and the experiment were in powder form.

Padjadjaran International Physics Symposium 2013 (PIPS-2013)
AIP Conf. Proc. 1554, 33-37 (2013); doi: 10.1063/1.4820277
978-0-7354-1180-7/$30.00

EXPERIMENTAL

The ACM from RWSD was prepared using our previous reported method [17]. Thermal properties of the products were carried out on a Mettler Toledo STAR from room temperature to 600 °C at a heating rate of 10 °C per minute under N_2 flow of 40 ml per minute min to prepare the suitable carbonization process. Green monolith (GM) of the SACG were prepared in a mould (20 mm in diameters) using 8 metric tons of compression force and then carbonized at several carbonization temperatures, namely 400, 500, 600, 700, 800 and 900 °C under N_2 atmosphere, to observe the effect of the carbonization temperature on the porosity characteristics of the ACM. After that, the samples were activated by CO_2 activation process at a temperature of 800 °C (heating rate of 10 °C per minute and flow rate of 1 liter per minute) for one hour. Finally, the entire ACM were polished into a desire thickness and then washed with a copious amount of distilled water. These ACM were labeled as ACM48, ACM58, ACM68, ACM78, ACM88 and ACM98. The first number after ACM corresponds to the carbonization temperature and the second activation temperature, respectively. If ACM48 referred, the sample was the one carbonized at 400 °C and CO_2 activated at 800 °C. After the optimum carbonization temperature have been understood, to continue improve the porosity of the ACM it has important follow with variation holding time of activation at optimum activation temperature namely 900 °C [18] for 1.5, 2.0 and 2.5 h with one step activation process.

The microporosity of the ACM was characterized using a conventional porosimeter ASAP 2000 micromeritics under a N_2 flow at -196 °C. From this experiment, by utilizing the BET and Dubinin-Radushkevich (DR) equations [19], the BET surface area and the micropore volume of the ACM can be obtained. The total pore volume of the sample was assumed as the liquid volume of adsorbate (N_2) at a relative pressure of 0.995. The morphological structures of the ACM were elucidated on a FESEM (Supra PV 55 model). The electrochemical performance of the ACM samples was investigated by cyclic voltammetry (CV) measurement in 1 M H_2SO_4 using a three-electrode testing cell. The working electrode were prepared by cutting an ACM in to a certain size of 1 cm^2 and weight 29 to 34 mg and detail experiment procedure based on our previous method [18]. The CV experiment was perform using a 1280 Solartron with a potential window of 0.1 to 1.0 V Vs reference electrode and the scan rate of 1 mV s^{-1} to 5 mV s^{-1}.

RESULTS AND DISCUSSION

Biomass, such RWSD, usually consists of hemicellulosa, cellulose and lignin. The pyrolysis of pra-carbonized RWSD could be attributed to the pyrolysis of the polymer. Fig. 1a shows the thermogravimatric analysis (TGA) and differential thermogravimatric analysis (DTGA) shown in Fig. 1b curve obtained from pyrolysis of RWSD under N_2 atmosphere. The TG decomposition curves for RWSD are shown the mass loss during the thermogravimetric analysis can be divided into stage. The first mass loss was verified by heating the material up to 220 °C, and this is due to moisture elimination. The second stage (220-370 °C), which corresponds to the primary carbonization, has a greater mass lose (ca.40%). This stage presents a considerably greater weight loss for the pra-carbonized RWSD, due to the elimination of volatile metters and tars. For this study, the active pyrolysis (weight loss of cellulose, hemicelluloses and lignin) of RWSD contained one stage (see the DTG curve in Fig. 1b). This corresponds to expected temperature range in which cellulose and lignin components in biomass are decomposed together [19-20]. The third stage was found in the 370-600 °C range, and indicates the decomposition of a structure with higher stability.

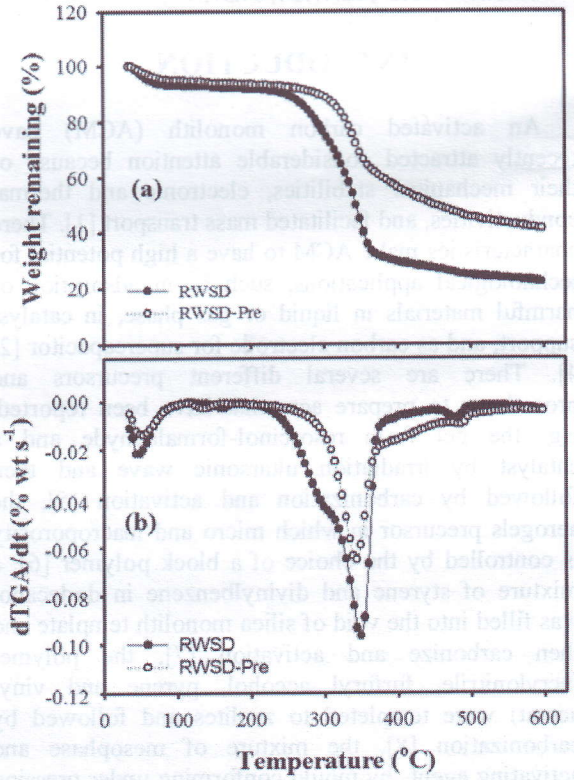

FIGURE 1. Thermal gravimetric analyses (TGA) (a) and derivative thermal gravimetric analyses (DTGA) (b) for RWSD before and after pre-carbonization process.

Fig. 2 show the N_2 adsorption/desorption isotherm plot for the samples ACM48 to ACM98. All of the samples have common typical microporous characteristic since all the plot exhibit a type-I [22] isotherm profile with a prominent plateau begin at very low pressure due to a successful formation of multilayer adsorbents on the pore volume of samples during adsorption process. However, the curve for the sample ACM68 seems to be well separated above that of other sample, indicating that the ACM have very much higher adsorption capacity. As can be seen in the Table 1, the value of surface area for this sample is almost double than that of other samples. Another different detail feature of the curve for the ACM68 is that a knee shape of the curve at low pressure reform is wider indicating that the ACM68 has higher volume of micropore.

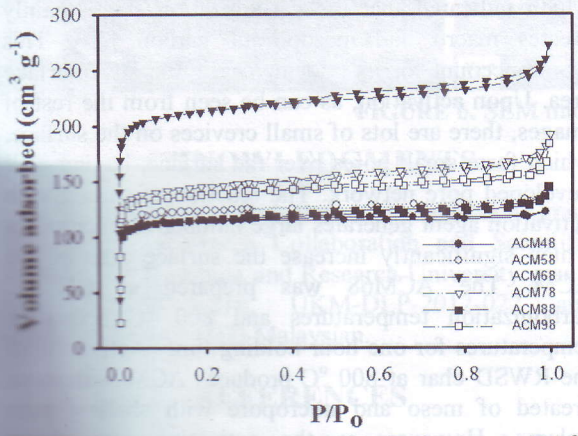

FIGURE 2. N_2 adsorption/desorption isotherms at -196 °C for ACM with varies carbonization temperatures.

TABLE 1. Porosity data for ACM with varies carbonization temperatures.

Sample	S_{BET} ($m^2 g^{-1}$)	S_{meso} ($m^2 g^{-1}$)	V_{micro} ($cm^3 g^{-1}$)	V_{meso} ($cm^3 g^{-1}$)	D (nm)
ACM48	345.91	34.38	0.160	0.028	3.305
ACM58	375.61	45.64	0.171	0.042	3.630
ACM68	733.99	57.54	0.307	0.101	2.224
ACM78	489.06	44.38	0.207	0.075	2.309
ACM88	390.79	27.05	0.168	0.047	2.210
ACM98	467.35	34.72	0.200	0.064	2.261

The highest S_{BET} value for the sample ACM 68 may be interpreted as due to the presence of higher volume of rudimentry pore in this monolitic char, which can optimally be expanded by CO_2 activation for the creation of new creation of new additional micropore in the sample. It is posible that below 600 °C such rudimentry pores are not yet completely formed and above this temperature the rudimentry pores are already "melted" or damage. Thereby these monolitic char producing less micropore after CO_2 activation.

Fig. 3 shows typical cyclic voltammogram of the entire sample measured at a scan rate of 5 mV s^{-1} for comparison. From the figure, it can be clearly seen that the ACM68 did exhibited the largest curve-area compare to the other samples. As has been earlier noted, the sample did have the highest porosity characteristic. Thus, facilitated an optimum diffusion process of the ionic charge in the bulk samples. Similar CV profile was also obtained for the other samples, such as ACM48, ACM58, ACM68, ACM78, ACM88 and ACM98. However, their related Faradic current density and the peak to peak separation were particularly lower compared to that of obtained in the sample ACM68. A complete measurement result of the CV of all the samples in a scan rate of 1 mVs^{-1} also has been recorded. Using the CV results, we calculated the specific capacitance of the sample. As in our previous report, the specific capacitance can be simply calculated by using the relation that has been reported [18]. The highest specific capacitance value as high as 32.13 F g^{-1} recorded ACM68 electrode.

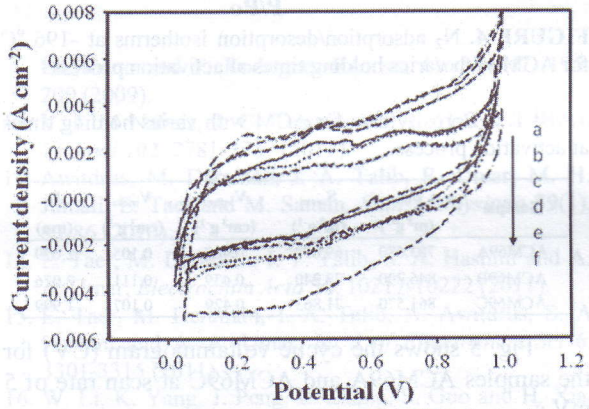

FIGURE 3. Cyclic voltammetry of ACM electrodes: a) ACM48, b) ACM58, c) ACM68, d) ACM78, e) ACM88 and f) ACM98.

In this context, one has chosen 600 °C as an optimum carbonization temperature to prepared monolithic char for further optimization surface area by varying activation and chosing a new activation at 900 °C. The choice of 900 °C is based on the data in ref [18]. Fig. 4 also shown that the increase of holding time 30 to 60 minutes, from 1.5 hours to 2 hours and 2.5 hours cause the adsorption capacity of the ACM to increase about 10%. The reason for this increase is well known, longer holding time creates more carbon-carbon dioxide reaction which can form fresh micropores, thereby leading to hingher surface area and micropore volume of the ACM. However, for futher increase in holding time, i.e. up to slightly higher than 2.5 hours, such a prosessive development of micropore did not occure since excessive occurrence of carbon-carbon dioxide reaction can

cause the breakage of pore walls and obviously followed by the collapse of ACM monolithic structure. Therefore this study suggests that the CO_2 activation condition that can preserve the monolithic form of ACM requires holding time less than 2.5 hours. Quantitavelly, the influence of varying the holding time on the porosity characteristic of the ACM is shows in Table 2.

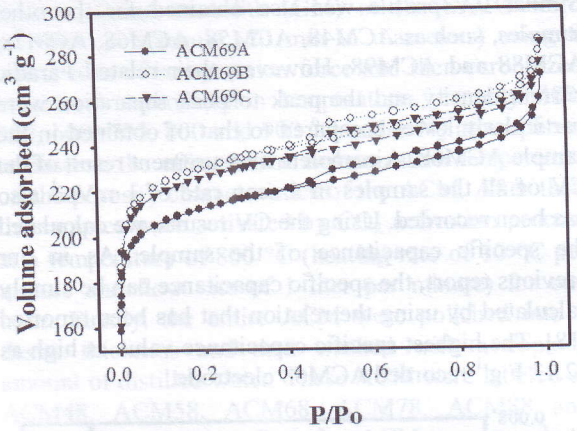

FIGURE 4. N_2 adsorption/desorption isotherms at -196 °C for ACM with varies holding times at activation process.

TABLE 2. Porosity data for ACM with varies holding times at activation process.

Sample	S_{BET} ($m^2 g^{-1}$)	S_{meso} ($m^2 g^{-1}$)	V_{mikro} ($cm^3 g^{-1}$)	V_{meso} ($cm^3 g^{-1}$)	D (nm)
ACM69A	783,680	69,010	0,407	0,105	2,079
ACM69B	846,290	73,240	0,439	0,111	2,076
ACM69C	861,570	71,863	0,429	0,107	1,999

Fig. 5 shows the cyclic voltammogram (CV) for the samples ACM69A and ACM69C at scan rate of 5 mV s^{-1}.

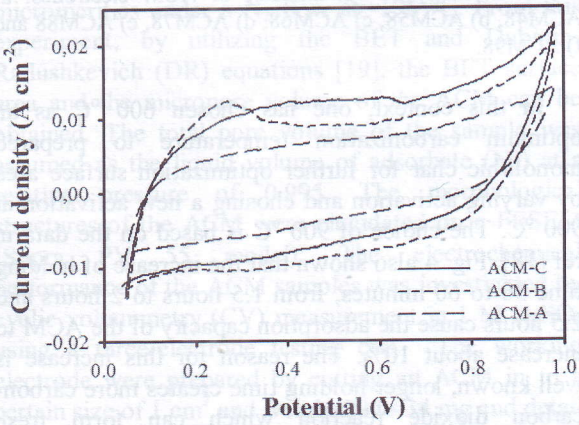

FIGURE 5. Cyclic voltammetry of ACM electrodes with varies holding times at activation process.

From the curves, it can also be clearly seen that the shape of the curve for the entire sample were similar, however the current density of ACM69C sample is the highest than the other samples. It is indicated by the enlargement in the CV area. It can be note here that the improvement in the current could be related to the increase in the surface area in the ACM as the porosity development during activation. This in turn may improve the proton diffusion and migration process in the bulk ACM. The highest CV area indicated the highest specific capacitance. The specific capacitance values for the ACM69A, ACM69B and ACM69C electrodes at scan rate 1 mV s^{-1} are 60.32, 75.61 and 90.72 F g^{-1}, respectively. The specific capacitance values are comparable with other biomass based electrodes such as durian shell [23] and waste coffee ground [24].

Fig. 6 shows SEM photographs of the RWSD char (CM6) and derivate ACM, respectively. As can be seen from the image CM6, the surface of primary char utilized for activation is planar with hole structure, which indicated that the carbonization stage mainly creates macro and mesoporous carbon [25]. This would account for its poor or negligible BET surface area. Upon activation, as can be seen from the rest of images, there are lots of small crevices on the surface, which form small pores over the surface, having well developed pore network. The reaction of carbon with activation agent generates large number of micropores which significantly increase the surface area of the ACM. The ACM68 was prepared at 600 °C carbonization temperatures and 800 °C activation temperatures for one hour holding time. Activation of the RWSD char at 800 °C produces ACM with more created of meso and micropore with shallow pore volume. However, as the activation temperature increase from 800 to 900 °C, the development of the pore structure is shown in ACM69 electrode. Small pore, transitional pore and large pore with different shape could also be clearly identified from this micrograph with deeper pore structure, which account for the higher BET surface area and micropore volume. In addition, these micrographs clearly show that ACM69C is more porous than ACM68, which has evenly distributed pores with high density.

Based on the evaluation on the entire experimental result, it can be concluded that the carbonization parameter especially carbonization temperature has a important part from all of process to created the highly porosity characteristic of ACM from RWSD. Based on the optimum carbonization temperature ca. 600 °C (ACM68 with BET surface area733 $m^2 g^{-1}$), it is one step to create the ACM with higher surface area (ACM69C with BET surface area 861 $m^2 g^{-1}$). Owing to its simple treatment procedure, the manipulation of the carbonization temperature may become a potential method for improving the porosity characteristic of ACM from the RWSD.

CONCLUSIONS

The effect of the carbonization temperature on the porosity of binderless ACM from RWSD has been studied. In typical process, by controlling the carbonization temperature, the porosity characteristic of the ACM can be effectively optimized. The optimum carbonization temperature has been obtained ca. 600 °C by surface area parameter (733 m^2 g^{-1}) at activation temperature 800 °C for one hour holding time. It is give simpler step to gate the higher surface area by determined proper activation condition (900 °C, 2.5 h holding time) namely 860 m^2 g^{-1}. In addition, simple preparation process and renewable precursor, the ACM from RWSD can be applied to variety application.

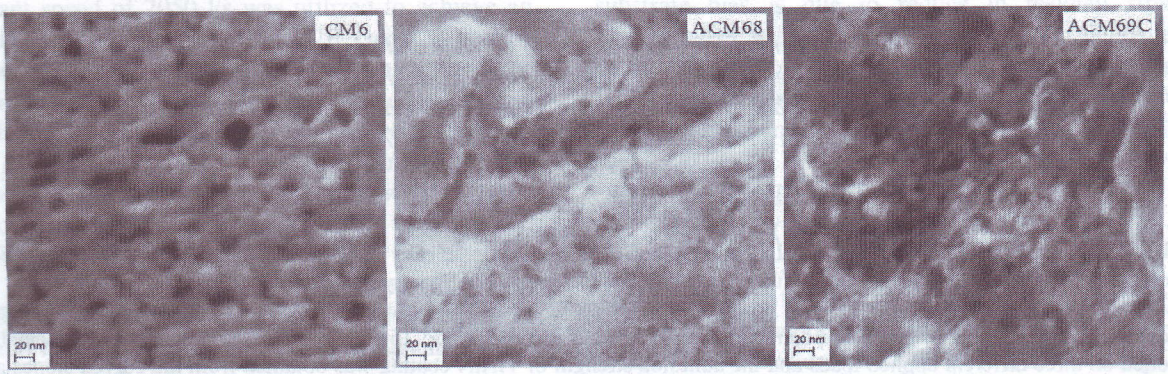

FIGURE 6. SEM micrograph for ACM electrodes.

ACKNOWLEDGMENTS

The authors acknowledge the research grant International Research Collaboration and Scientific Publication, Indonesia and Research University grants (UKM-GUP-2011-216, UKM-DLP-2012-022 and UKM-DLP-2012-023) Malaysian.

REFERENCES

1. A. Stein, Z. Y. Wang and M. A. Fierke. *Adv Mater* **21**, 265-293 (2009).
2. D. Tang, Z. Zheng, K. Lin, J. F. Luan and J. B. Zhang, *J. Hazardouz Mater* **143**, 49-56 (2007).
3. W. Z. Shen, H. Wang, R. G. Guan and Z. J Li, *Colloids and surface A: Physicochemical and enggineering aspects* **331**, 263-267 (2008).
4. A. Carcia-Gomez, P. Miles, T. A. Centeno and J. M. Rojo, *Electrochim Acta* **55**, 8539-8544 (2010).
5. A. Siyasukh, P. Maneeprom, S. Larpkiattaworn, N. Tonanon, Tanthapanichakoon, H. Tamon and T. Charinpanikul, *Carbon* **46**, 1309-1315. (2008).
6. M. C. Gutierrez, F. Pico, F. Rubio, J. M. Amarilla, F. J Palomares, M. L. Ferrer, F. Del Monte and J. M. Rojo, *J. Mater Chem* **19**, 1236-1240 (2009).
7. L. -Y. Xu, Z. -G. Shi and Y. -Q. Feng, *Micro and Meso Mater* **115**, 618-623 (2008).
8. C. J. Meyers, S. D. Shah, S. C. Patel, R. M. Sneeringer, C. A. Bessel, N. R. Dollahon, R. A. Leising and E. S Takeuchi, *J. Phys Chem B* **105**, 2143-2152 (2001).
9. J. M. Ramos-Fernandez, M. Martinez-Escandell and F. Rodriquez-Reinoso, *Carbon* **46**, 384-389 (2008).
10. R. Ubago-Perez, F. Carrasco-Marin, D. Fairen-Jimenez and C. Moreno-Castilla, *Micro and Meso Mater* **92**, 64-70 (2006).
11. V. Ruiz, C. Blanco, R. Santamaria, J. M. Ramos-Fernandez and M. Martinez-Escandell, A. Sepulveda-Escribano and F. Rodriguez-Renoso, *Carbon* **47**, 195-200 (2009).
12. V. J. M Nabais, J. G. Teixeira and I. Almeida, *Biores Technol* **102**, 2781-2787 (2011).
13. Awitdrus, M. Deraman, I. A. Talib, R. Omar, M. H. Jumali, E. Taer and M. Saman, *Sain Malaysiana* **39**(1), 83-86 (2010).
14. E. Taer, M. Deraman, I. T. Talib, S. A. Hashmi and A. A. Umar, *Electrochim Acta* **56**, 10217-10222 (2011).
15. E. Taer, M. Deraman, I. A. Talib, A. Awitdrus, S. A Hashmi and A. A. Umar, *Int J of Electrochem Sci* **6**, 3301-3315 (2011).
16. W. Li, K. Yang, J. Peng, L. Zhang, S. Guo and H. Xia, *Industrial Crops and Products* **28**, 190-198 (2008).
17. M. Deraman, R. Omar, S. Zakaria, I. R. Mustapa, M, Talib, N. Alias and R. Jaafar, *J. Mater Sci* **37** (16), pp. 3329-3335 (2002).
18. E. Taer, M. Deraman, I. A. Talib, A. A. Umar, M. Oyama and R. M. Yunus, *Curr Appl Phys* **10** 1071–1075 (2010).
19. P. A. Webb and C. Orr, *Micromeritiecs Instrument Corp* Norcross: Georgia, USA,. (1997).
20. R. M. Suzuki, A. D. Andrade, J. C Sousa and M. C Rollemberg, *Biores. Technol* **98**, 1985-1991 (2007).
21. A. Aworn, P. Thiravetyan and W. Nakbanpote, *Colloids. Surf.* A **333**, 19-25 (2009).
22. K. S. W. Sing, D. H. Everret, R. A. W. Haul, L. Moscou, R. A. Pierotti, J. Rouquerol and T. Siemieniewska, *Pure Appl Chem* **57**, 603 (1985).
23. L. K. Ong, A. Kurniawan, A. C. Suwandi, C. X. Lin, X. S. Zhao and S.Ismadji, *Progress in Natural Science: Materials International* **22(6)**, 624-630 (2012).
24. T. E. Rufford., D. Hulicova-Jurcakova., E. Fiset., Z. Zhu. and G. Q. Lu., *Electrocem. Com* **11**, 974–977. (2009).
25. R. Arriagada, R. Garcia, M. Molina-Sabio and F. Rodriguez-Reinoso. *Micropor Mater* **8**, 123–30 (1997).

Composite Electrodes of Activated Carbon Derived from Cassava Peel and Carbon Nanotubes for Supercapacitor Applications

E. Taer[1,*], Iwantono[1], M. Yulita[1], R. Taslim[1], A. Subagio[2], Salomo[1] and M. Deraman[3]

[1]*Department of Physics, University of Riau, 28293 Simpang Baru, Riau, Indonesia*
[2]*Department of Physics, Dipenegoro University, 50275 Tembalang-Semarang, Central Java, Indonesia*
[3]*School of Applied Physics, Faculty of Science and Technology, Universiti Kebangsaan Malaysia, 43600 Bangi, Selangor, Malaysia*
[*]*erman_taer@yahoo.com*

Abstract. In this paper, a composite electrode was prepared from a mixture of activated carbon derived from pre-carbonization of cassava peel (CP) and carbon nanotubes (CNTs). The activated carbon was produced by pyrolysis process using $ZnCl_2$ as an activation agent. A N_2 adsorption-desorption analysis for the sample indicated that the BET surface area of the activated carbon was 1336 $m^2 g^{-1}$. Difference percentage of CNTs of 0, 5, 10, 15 and 20% with 5% of PVDF binder were added into CP based activated carbon in order to fabricate the composite electrodes. The morphology and structure of the composite electrodes were investigated by scanning electron microscopy (SEM) and X-ray diffraction (XRD) techniques. The SEM image observed that the distribution of CNTs was homogeneous between carbon particles and the XRD pattern shown the amorphous structure of the sample. The electrodes were fabricated for supercapacitor cells with 316L stainless steel as current collector and 1 M sulfuric acid as electrolyte. An electrochemical characterization was performed by using an electrochemical impedance spectroscopy (EIS) method using a Solatron 1286 instrument and the addition of CNTs revealed to improve the resistant and capacitive properties of supercapacitor cell.

Keywords: Activated carbon, Supercapacitor, Cell resistance, Carbon nanotubes.
PACS: 81.05.U-, 82.47.Uv, 87.15.Vc, 88.30.rh

INTRODUCTION

Supercapacitor or electrochemical double layer capacitor (EDLCs) is an energy storage device that uses to store and release energy [1]. Supercapacitor consists of electrodes, separator, current collector and electrolyte. The supercapacitor performances (energy and power density) mostly depend on the electrode and electrolyte properties. Many carbon based materials have been developed as electrodes for EDLCs, such as graphene, carbon nanotubes (CNTs), carbon aerogels and activated carbon [2]. The activated carbon is commonly used as electrode material for some advantages such as high surface area, wide availability and low cost production compared to other carbon based materials. Recently, many studies focus on EDLCs to produce activated carbon electrodes from biomass waste materials by chemical and physical activation process.

Biomass materials as carbon electrode precursor for supercapacitor application by using chemical and physical activation methods has been widely studied and reported [3]. Ismanto et al have used cassava peel (CP) to produce supercapacitor electrodes by using chemical activation process of KOH activation agent [4]. The activated carbon electrode with surface area and capacitance specific obtained of 1352 m^2g^{-1} and 153 Fg^{-1}, respectively. A $ZnCl_2$ activation agent has also been used in chemical activation process for CP and had a surface area as high as 1500 m^2g^{-1} [5]. In this paper a high surface area activated carbon from CP waste of Riau local area by using the $ZnCl_2$ activation agent will be demonstrated. The porosities properties of CP based activated carbon were investigated by using N_2 adsorption-desorption method. The influence of CNT addition in CP based activated carbon electrodes for improving supercapacitive properties such as equivalent series resistance and specific capacitance will be discussed in detail, the micro-crystallite and morphologies properties of the composite CP activated carbon and CNT electrode were also studied by X-ray diffraction and scanning electron microscopy measurement.

Padjadjaran International Physics Symposium 2013 (PIPS-2013)
AIP Conf. Proc. 1554, 70-74 (2013); doi: 10.1063/1.4820286
LLC 978-0-7354-1180-7/$30.00

EXPERIMENTAL

CP was first pre-carbonized and followed by ball-milling and sieving to obtain carbon grains (CG) with particle size of less than 103 micron [6]. The CG was then mixed with an activation agent of ($ZnCl_2$) with a weight ratio of 1:1.5. Two hundred ml of distilled water was added into 100 g of the mixture materials and magnetically stirred in 2 hours before drying for 24 hours. Carbonization of the dried mixture materials was done at 600 °C under N_2 atmosphere (flow rate of 1.5 litter per minute) and activated carbon powder (ACP) produced were washed using 1% HCl and distilled water until the pH of distilled water turns to neutral, and finally dried it at a temperature of 100 °C for 24 hours before sieving to obtain an ACP with particle size of less than 103 micron.

Five different electrodes in coin shape were prepared from the ACP and CNTs (Nanostructured & Amorphous Materials.Inc), by using a PVDF (Acros Organics) adhesive as a binder material. Varies weight of these materials shows in Table 1 was carried out by ball-milling technique for 1 hour. Fabrication of an electrode in the form of sheet ~0.2 mm thickness from these materials was manually done using a mortar [7]. The produced sheet was then cut using coin shaped mold to get an electrodes with diameter of 15 mm. The coin shaped electrodes were followed by heating at 75 °C for 24 hours and the electrode was then used to fabricate a symmetrical supercapacitor cells based on our previous method [8,9].

TABLE 1. Electrode compositions.

Electrodes	Compositions by weight (%)		
	ACP	PVDF	CNT
A	95	5	0
B	90	5	5
C	85	5	10
D	80	5	15
E	75	5	20

The porosity characteristics such as BET surface area (S_{BET}), mesopore surface area (S_{meso}), micropore surface area (S_{mic}), external surface area (S_{ext}), average pores diameter (D_{av}) of ACP were determined by an adsorption-desorption isotherm experiment (N_2 gas at 77 K) using an accelerated surface area and a porosimeter system (ASAP 2010 micromeritic). The BET surface area was calculated from the isotherms using the BET equation [10]. In this experiment, the cross-sectional area of a nitrogen molecule was assumed to be 0.162 nm2. The Dubinin-Radushkevich equation was used to calculate the micropore volume from which the micropore surface area was then determined [10]. A surface microstructure of the electrodes was characterized by a FESEM (SUPRA PV 55 model). The diffraction patterns were obtained using a diffractometer (Bruker AXS D8 advance) that employed CuKα radiation with a 2θ range from 0o to 70o.The performance of fabricated supercapacitor cells was investigated by an electrochemical impedance spectroscopy measurement using Solartron 1286 conducted at 10 mV over a frequency range of 100 kHz to 10 mHz.

RESULT AND DISCUSSION

Fig. 1 show an adsorption-desorption curve for the CP based ACP. This curve is typical behavior for a type IV material based on IUPAC classification [11], indicating the CP based activated carbon comprising both micro-pores and meso-pores. The pore size distribution can be observed in Fig. 1b.

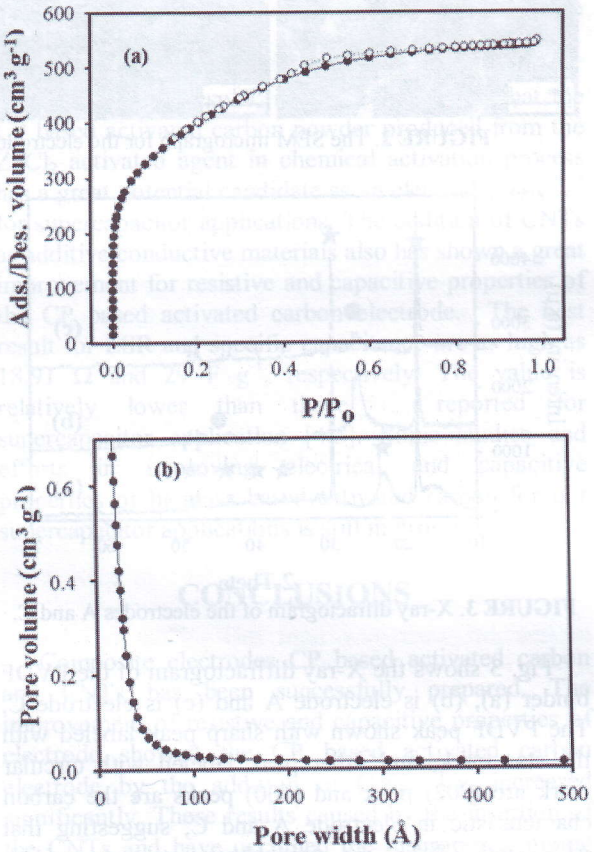

FIGURE 1. N_2 gas adsorption-desorption (a) and (b) pore size distribution of activated carbon from CP.

TABLE 2. Porosity data for CP based the ACP.

S_{BET} (m^2g^{-1})	S_{Mikro} (m^2g^{-1})	S_{Meso} (m^2g^{-1})	S_{Ext} (m^2g^{-1})	D (Å)
1374.27	185.17	1090.86	1189.10	24.41

The porosity properties are listed in Table 2. From the table shows the CP based activated carbon is very

porous material with mesopores as a main contributor to the S_{BET} value (almost 80%). A similar result was observed for activated carbon powder used the $ZnCl_2$ activated agent from biomass precursor with the optimum S_{BET} value as high as of 1489 $m^2 g^{-1}$ (89% mesopores) for the bagasse based ACP [12]. The study of *camellia oleifera* shell based ACP found the maximum S_{BET} as high as of 2086 $m^2 g^{-1}$ (87% mesopore) [13]. Our results show a messopores characteristic than those reported by Ismanto *et al.* [4].

Fig. 2 shows the SEM micrographs for electrodes A (2a and 2c) and C (2b and 2d) with different magnifications. The micrograph 2(a) shows the sizes of CP activated carbon particle are 1-2 μm in range with the presence of open macropores between the carbon particles. The addition of 10% CNTs (Fig. 2b), can be observed that the open macropore occupied by CNTs which distribute homogeneously. Meanwhile, Fig. (2b and 2c) are clearly seen that the surface morphology of the CP carbon electrode and the CNTs composite electrodes. The presence of CNTs should improve the resistive and capacitive properties of the CP based activated carbon electrode and will be discussed detail in section of cell properties discussion.

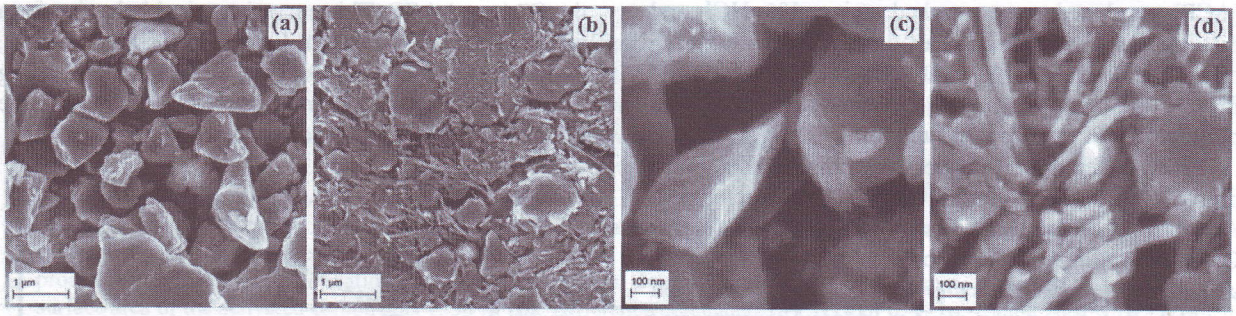

FIGURE 2. The SEM micrograph for the electrodes A (a and c) and C with different magnification (b and d).

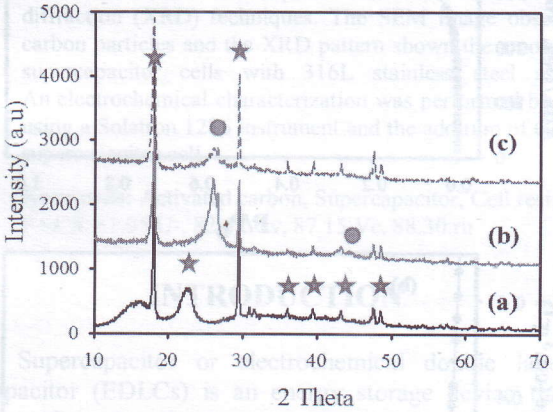

FIGURE 3. X-ray difractogram of the electrodes A and C.

Fig. 3 shows the X-ray diffractogram of the PVDF binder (a), (b) is electrode A and (c) is electrode C. The PVDF peak shown with sharp peak labeled with the star mark, and other peak labeled with circular mark are (002) peak and (100) peaks are the carbon characteristic in electrode A and C, suggesting that ACP and CNTs are amorphous structures [14]. However, for the electrode C, the peak (002) decreases sharply and the peak (100) is also very weak, this indicates that the addition of CNTs causes localized defects on ACP particles and suggest that composite electrode ACP and CNTs are more amorphous structures, which leads improve the porosity properties of the electrode. Finally the addition of CNTs may improve the electrical and capacitive properties of the electrode.

The electrochemical (resistive and capacitive) properties of the composite electrodes were obtained by an electrochemical impedance spectroscopy (EIS) measurement. Fig. 4 shows the Nyquist plot of different CNTs addition electrodes in the frequency region of 10 mHz to 1 MHz, the inset shows the Nyquist plot in frequency region of 10 mHz to 1 kHz. The figure clearly shows that the plot consists of three different regions, namely: a semi-circular section, a line with a slope of 45° and a line perpendicular to the axis of the real impedance (Z '). The first intersect of the curve with real impedance axis (Z ') contributes to the electrolyte resistance, contact resistance between the current collectors and electrodes (Rs), which is formed at a high frequency region (1MHz). A polarization resistance (Rp) was generated by fit of the Nyquist plot, the extended of the plot that intersects with the Z' axis is namely as Rp . The calculation of Rs, Rp and ESR values that are based on data in the Fig. 4 was carried out using standard Z-View software by the fitting technique [9]. The resistive properties of the cells (Rs, Rp and ESR (Rs-Rp)) are tabled in the Table 3.

TABLE 3. Resistive properties of CP activated carbon based with different CNTs percentages.

Sample Code	R_s (Ω)	R_p (Ω)	ESR(Ω)
A	19.33	4264.40	4283.70
B	3.70	645.53	641.83
C	2.93	84.62	81.70
D	1.39	20.30	18.91
E	0.68	13.61	12.92

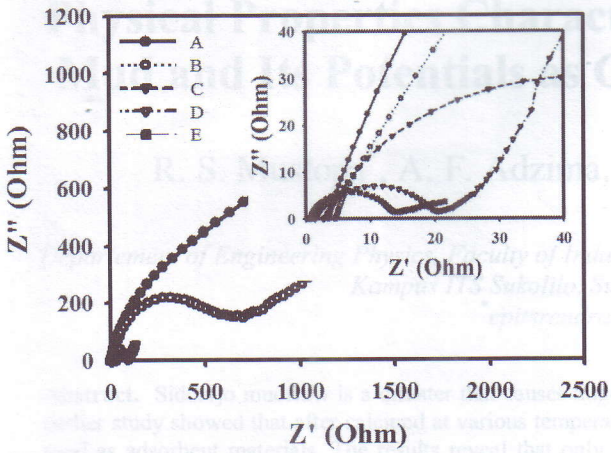

FIGURE 4. Nyquist plot of the supercapacitor cell with difference percentage addition of CNTs electrodes.

From the Table 3, the influence of CNTs in CP based activated carbon electrode is clearly improved the electrical properties of the cells. The increasing of CNTs addition in the carbon electrode is proportional to the decrease of cell resistance properties. It is clearly shown that the values of R_s, R_p and ESR decreased significantly for the samples after CNTs additions. For example, the value of Rs, Rp and ESR are reduced significantly after 20% CNTs addition such as; from 19.33 Ω to 0.68 Ω, from 4264 Ω to 13.61 Ω and from 4283 Ω to 12.92 Ω, respectively. The improving Rs related to the closing of the open macro-pores among the carbon particles and improving the interfacial contact between the current collector and electrode and reducing the Rs value. The decrease of the electrode resistance value (Rp) is also observed by mean of the effect of the CNTs additions. This phenomenon has been expected previously since CNTs are good conductive materials. The insertion of CNTs between the carbon particles which fill in the open macropore has been giving a bridge for the electron transport that will lead reducing the electrode resistance. A reduction in ESR is due to the reducing of R_s and R_p. In conclusion, the addition of CNTs to the samples gave great affects on the resistance properties of supercapacitor cell.

By using a relation of $C_{sp} = -1/\omega Z''$ [8], the specific capacitance of the composite electrodes can be obtained from the Nyquist plot (Fig. 4). The specific capacitance versus frequency is shown in the Fig. 5. The CNTs addition has increased the specific capacitance values with significant increase were observed, especially at low frequency region (10 mHz). It is because the ions of electrolyte can be easily diffuse into the carbon pores in long cycle time and consequently more double layer of the ions-electrons pairs inform at the interface of the carbon surface and the electrolyte. Improving the specific capacitance is directly proportional to the addition of CNTs, it is due to the reduction in cell resistance properties that have been described in the previous part.

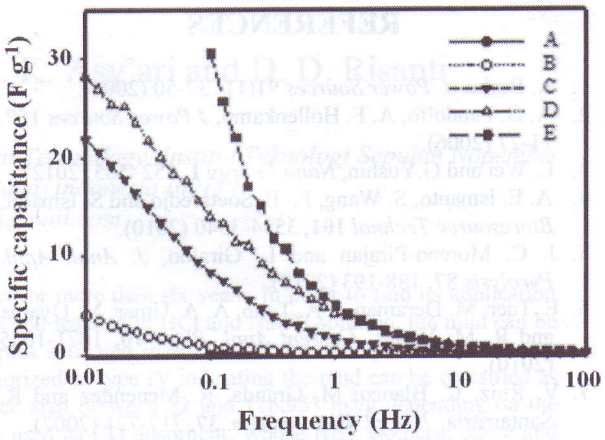

FIGURE 5. The specific capacitance values versus frequency for the supercapacitor cell with difference percentage addition of CNTs electrodes.

Based on the results, it can be concluded that the CP based activated carbon powder produced from the $ZnCl_2$ activated agent in chemical activation process has a great potential candidate as an electrode material for supercapacitor applications. The addition of CNTs as additive conductive materials also has shown a great improvement for resistive and capacitive properties of the CP based activated carbon electrode. The best result for ESR and specific capacitance are as high as 18.91 Ω and 29 F g^{-1}, respectively. The value is relatively lower than those reported for supercapacitor application [4,5]. Some studies and efforts in improving electrical and capacitive properties of biomass based activated carbon for our supercapacitor applications is still in progress.

CONCLUSIONS

Composite electrodes CP based activated carbon and CNTs has been successfully prepared. The improvement of resistive and capacitive properties of electrode showed the CP based activated carbon electrode by the addition of CNTs has increased significantly. These results caused by the insertion of the CNTs and have occupied the macropores among the carbon particles. Finally, the composite electrode has been prepared by the simple and easy preparation method.

ACKNOWLEDGMENTS

The authors acknowledge the research grant International Research Collaboration and Scientific Publication, Indonesia and Research University grants

(UKM-GUP-2011-216, UKM-DLP-2012-022 and UKM-DLP-2012-023) Malaysia.

REFERENCES

1. A. Burke. *J Power Sources* **91**(1), 37-50 (2000).
2. A. G. Pandolfo, A. F. Hollenkamp, *J Power Sources* **157**, 11-27 (2006).
3. L. Wei and G.Yushin, *Nano Energy* **1**, 552–565 (2012).
4. A. E. Ismanto, S. Wang, F. E. Soetaredjo and S. Ismadji, *Bioresource Technol* **101**, 3534-3540 (2010).
5. J. C. Moreno-Pirajan and L. Giraldo, *J. Anal. Appl. Pyrolysis* **87**, 188-193 (2010).
6. E. Taer, M. Deraman, I. A. Talib, A. A. Umar, M. Oyama and R. M. Yunus, *Current Appl. Phys.* **10**, 1071-1075 (2010).
7. V. Ruiz, C. Blanco, M. Granda, R. Menendez and R. Santamaria, *J. Appl. Electrochem.* **37**, 717-721 (2007).
8. E. Taer, I. M. Deraman, I. A. Thalib, A. Awidrus, S. A. Hashmi and A. A. Umar, *Int. J. Electrochem. Sci.* **6**, 3301-3315 (2011).
9. E. Taer, M. Deraman, I. A. Talib, S. A. Hashmi and A. A. Umar, *Electrochimica Acta* **56**, 10217-10222 (2011).
10. P. A. Webb and C. Orr, *Analytical Methods in Fine Particle Technology*, Georgia: Micromeritiecs Instrument Corp (1997).
11. K. S. W. Sing, D. H. Everret, R. A. W. Haul, L. Mouscou, R. A. Pierotti, J. Rouquerol and T. Siemieniewska, *Pure & Appl. Chem.* **57**, 603-619 (1985).
12. W. -J. Si, X. -Z. Wu, W. Xing, J. Zhou and S. -P. Zhuo, *J. Inorganic Mater.* **26** (1), 107-112 (2011).
13. J. Zhang, L. Gong, K. Sun, J. Jiang and X. Zhang, *J. Solid State Electrochem.* **16**, 2179–2186 (2012).
14. R. Farma, M. Deraman, A. Awitdrus, I. A. Talib, E. Taer, N. H. Basri, J. G. Manjunatha, M. M. Ishak, B. N. M. Dollah and S. A. Hashmi, *Bioresource Technol.* **132**, 254–261 (2013).

Synthesis of Silver Nanosheets onto Solid Substrates by using Seed-Mediated Growth Method

Iwantono[1,*], E. Taer[1], A. A. Umar[2] and T. T. Saputrina[1]

[1]*Department of Physics, Riau Uniersity, Jl. H.R. Soebrantas Km 12.5 Tampan Pekanbaru 28293, Riau, Indonesia*
[2]*Institute of Microengineering and Nanoelectronics, Universiti Kebangsaan Malaysia, 43600 Bangi, Malaysia*
* *iwan_tono@yahoo.co.uk*

Abstract. Silver nanosheets, with average size tunable from 30 to 100 nm, have been synthesized onto solid substrates by using seed-mediated growth method. The growth of silver nanosheets have been carried out at temperature of 30°C in the presence of a binary surfactant mixture: cetyl trimethyl ammonium bromide (CTAB) and poly-vinyl pyrrolidone (PVP) with their various concentrations. The effect of concentration of the surfactants on the grown silver nanosheets were evaluated. Characterizations of the samples have been performed by using UV-Vis spectroscopy, X-ray diffraction (XRD) and field-emission scanning electron microscope (FESEM). UV-Vis spectra showed that the silver nanoparticles have grown with a various geometrical forms. XRD results confirmed that the presence of two peaks at 2θ: 38.119° and 44.305° indicated the silver nanosheets, with their crystal orientation of (111) and (200). FESEM images of the best samples showed the edge-length size of silver nanosheets was dominated in the range of 30-100 nm, with various morphologies of nanosheets, such as triangular, hexagonal and spherical shapes.

Keywords: Silver nanosheets, structure, UV-Vis, XRD, FESEM.
PACS: 62.23.Kn, 61.46.Df

INTRODUCTION

Silver nanoparticles of different shapes, such as cubes and octahedrons [1,2], tetrahedrons [3], wires/rods [4,5] and plates/sheets) have attracted high research interest, due to their unique and tunable optical properties, as well as their wide potential applications, such as optical probes, optical labels, chemical and biological sensors [6]. Among them, two-dimensional (2-D) silver nanosheets have special attracted attention in the past decade [7], including triangular plates/sheets [8], nanodisc [9], and hexagonal plates. The morphology and size of silver nanoparticles are important aspects that relate to their properties and applications. Hence, the study of size and morphology of silver nanoparticles become one of focusing aspect of research on the materials.

Synthesis of nanoplates is generally performed by transformation of spherical nanoparticles into nanoplates by using photo-induced methods [10]. Simpler method used to synthesis of nanoplates is seed-mediated growth method [11,12]. Hexagonal silver nanoplates have grown by using sulphuric acid [13] and urea [14] as a modifier. In this current work, we use ascorbic acid and binary surfactants: Polyvinylpyrrolidone (PVP) and *Cetyl-trimethyl-ammonium bromide* (CTAB) in order to vary shapes of silver nanoplates/nanosheets.

EXPERIMENTAL PROCEDURES

Materials

Silver nitrate ($AgNO_3$), trisodium citrate ($C_6H_5Na_3O_7$), sodium borohydride ($NaBH_4$), ascorbic acid ($C_6H_8O_6$), Poly-vinyl-pyrrolidone (PVP) and *Cetyl-trimethyl-ammonium bromide* (CTAB) were all purchased from Sigma-Aldrich. In order to synthesis of silver nanosheets, all the chemicals were made into solution. All the solutions were prepared using deionized (DI) water.

Preparation of Silver-Seed

A standard procedure for the synthesis of silver-seed was as follows: 0.5 mL 0.01 M AgNO3 solution and 0.5 mL 0.01 M trisodium citrate were added to 20 mL DI water, solid substrate then was immersed into the seed-solution and the solution was kept under cold condition for about 30 min. After that, 0.5 mL of 0.1 M $NaBH_4$ solution was added to the mix solution, and then kept them for about 1 h before using as seed.

Padjadjaran International Physics Symposium 2013 (PIPS-2013)
AIP Conf. Proc. 1554, 79-82 (2013); doi: 10.1063/1.4820288
3-0-7354-1180-7/$30.00

From this approach, spherical nanoseed of size ca. 3-5 nm can be grown on the substrate surface. The shape and size stability was achieved by the presence of trisodium citrate capping agent.

Preparation of Silver-Nanosheets

Growth solution of silver nanosheets consists of 0.01 M $AgNO_3$ (a variety volumes), 0.1 mL 0.1M ascorbic acid, 10 mL CTAB (a variety concentrations) and 10 mL PVP (a variety concentrations). Then 20 µL NH_3 was added to the solution. These solutions were then kept at room temperature for about 4h.

The growth process of silver nanosheets on the solid substrates was performed by immersing the substrates into a glass tube that contained the growth solution for about 4 h. The CTAB and PVP here are the surfactants molecules that have function both as morphology and aggregation controllers.

Characterizations

The UV-Visible optical absorption spectroscopy was performed using UV-160 Lamda 900 (Perkin Elmer) spectrophotometer. In order to characterize the structural growth of the silver nanosheets on the solid substrates, the X-ray diffraction methods using an XRD D8 Advance (Bruker) with Cu KR irradiation operated at 50 kV and 300 mA and a scan rate as low as 2 degrees per minute were performed. The morphology of the silver nanosheets growth was characterized using a field-emission scanning electron microscopy (FESEM) with SUPRA 55VP instrument.

RESULTS AND DISCUSSION

Morphology and Structure of Silver-Nanosheets

Prior to studying the surfactant effect, the optimum $AgNO_3$ concentration for Ag nanosheet formation was sought. The morphologies of the silver-nanosheets were observed by field-emission scanning electron microscopy (FESEM). The FESEM images of the silver-nanosheets grown on the ITO substrates that prepared using the seed-mediated growth are shown in Fig. 1. It was clearly shown that almost all of the surface area of substrate (more than 85%) was covered by silver nanosheets in all samples with different volume (0.5 mL, 0.8 mL, 1 mL and 1.5 mL) of silver ($AgNO_3$) solutions. The plate/sheets-like morphology of the samples, including triangular, hexagonal, truncated-hexagonal, trapezium, circular and irregular-sheets were also observed.

Fig. 2 shows the high-magnification (50.000X) FESEM images of the samples. It was found clear shapes of triangular, hexagonal, truncated-hexagonal, trapezium, circular and irregular-nanosheets observed in all samples. It was also shown that among the samples, the sample (b) of 0.8 mL silver solution has the most number of particles compared to other samples. The edge-length size of the silver nanosheets/plates was observed to be in the range of 30 - 200 nm for the samples of 0.8 and 1.0 mL silver solution (sample B and C). Whereas, bigger particles with the edge-length size in the range of 200-400 nm were obtained from the samples of 0.5 and 1.5 mL of silver solutions (sample A and D).

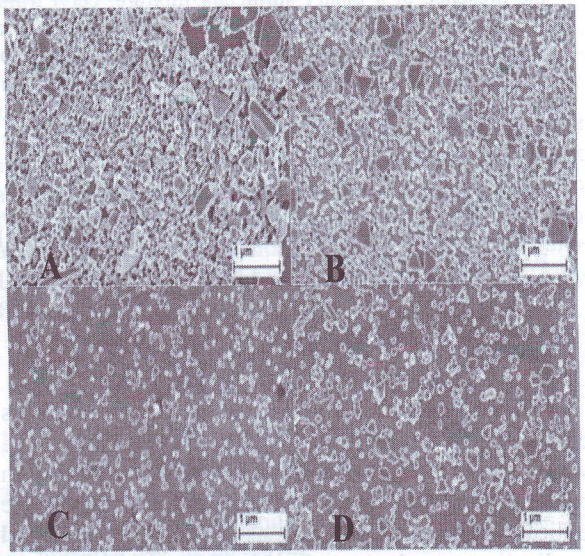

FIGURE 1. FESEM images of the silver nanosheets grown on ITO with volume of $AgNO_3$ (A) 0.5 mL, (B) 0.8 mL, (C) 1.0 mL and (D) 1.5 mL.

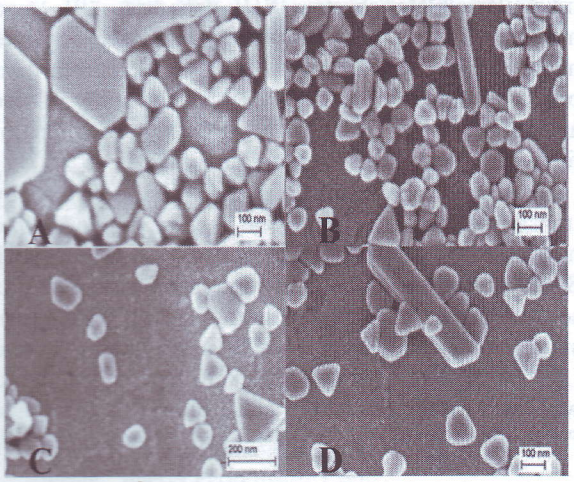

FIGURE 2. High-magnification (50.000X) FESEM images of the samples with volume of $AgNO_3$ (A) 0.5 mL, (B) 0.8 mL, (C) 1 mL and (D) 1.5 mL.

Individual silver-nanosheets of triangular, hexagonal, truncated-hexagonal, trapezium, circular and irregular-sheets are shown in Fig. 3. As can be seen that the size of the triangular, truncated-hexagonal, trapezium and irregular-sheets is about 100-200 nm in the edge-length. Whereas, more bigger size of silver nanosheets was observed to be the hexagonal-sheets, which was more than 500 nm in the edge-length.

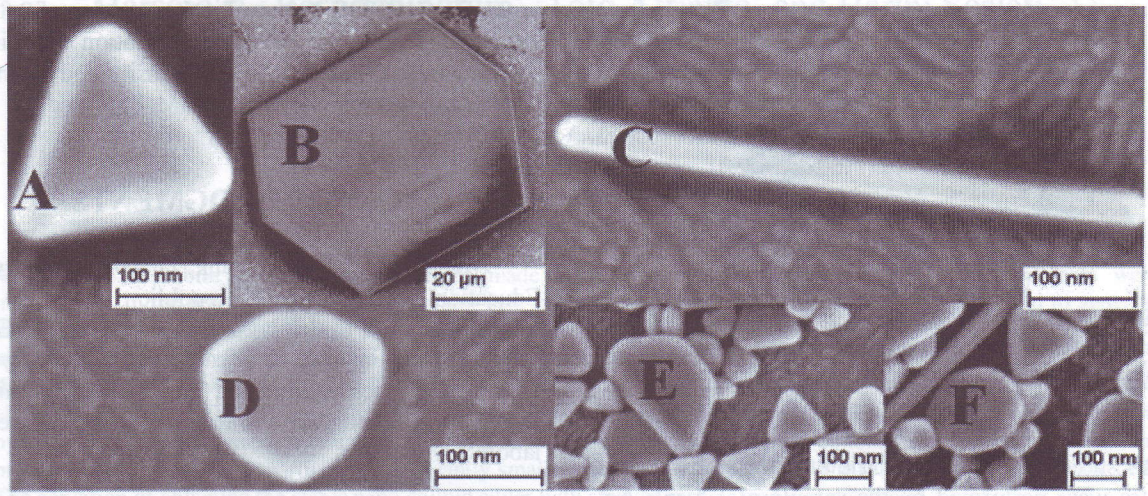

FIGURE 3. Individual silver-nanosheets (A) triangular (B) hexagonal (C) truncated-hexagonal (D) irregular-sheet (E) trapezium (F) circular.

The X-ray diffraction was carried out in order to determine the phase and purity of the samples. X-ray diffraction pattern of the silver-nanosheets (Fig. 4) shows that the peaks (38.119° and 44.305°) are assigned to the diffractions from the (111) and (200) planes of face-centre cubic symmetry of Ag (JCPDS No. 01-087-0717), respectively. In addition, there was no other impurity phase that was detected.

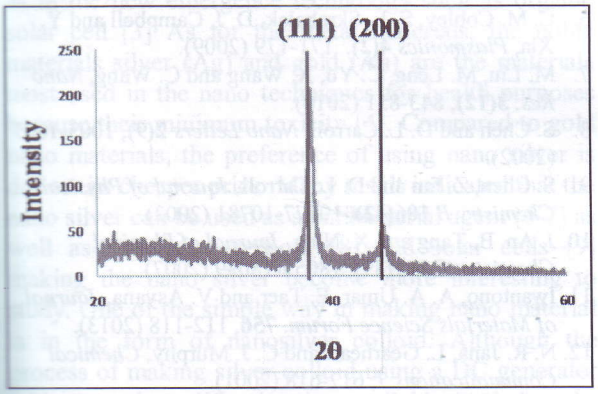

FIGURE 4. XRD pattern of the silver-sheets grown on ITO.

Effect of Surfactant on the Morphology and Structure of Silver-Nanosheets

The effect of concentration of surfactants on the morphology and structure of the products was evaluated by UV-VIS spectroscopy. Fig. 5 shows the UV-Vis spectra of the samples of silver nanosheets with different concentration of CTAB (150, 120, 100, 80 and 50 mM) at the same concentration of 0.8 mM PVP. The figure exhibits two peaks absorptions obtained from all samples, although the sample of 150 mM (a) shows weak peaks. Among them, the 50 mM CTAB sample produces the strongest absorption peaks, and this then was chosen as the best sample for further treatment.

The two absorption peaks at about 420 nm and 520 nm are contrary to a single SPR band for spherical silver nanoparticles. These two peaks are attributed to sheets-like silver nanoparticles. The number of peaks correlate with the number of ways the free electron oscillated. The strong peak at 420 nm is related to the Transverse Surface Plasmon Resonance (T-SPR), resonance toward the short axis, meanwhile the broad peaks at around 520 nm are due to Longitudinal Plasmon Resonance (L-SPR), a resonance toward the longer axis.

As can be seen from the Fig. 5, the spectrum of 50 mM CTAB sample has strongest absorption peak, due to the highest density of silver nanosheets compared to the other samples. On the other hand, the weakest peak of absorption spectrum from 150 mM CTAB sample, indicate the lowest density of silver nanoparticles grown on the sample.

UV-Vis spectra of the silver nanosheets with different volume of silver solution (0.5 mL, 0.8 mL, 1.0 mL and 1.5 mL) at the best concentration of binary surfactants of 0.8 mM PVP and 50 mM CTAB are shown in Fig. 6.

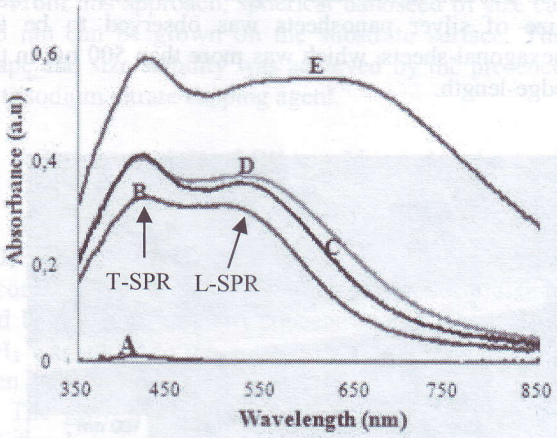

FIGURE 5. UV-Vis spectra of the silver nanosheets with 0.8 mM PVP and various concentrations of CTAB. (A) 150 mM (B) 120 mM (C) 100 mM (D) 80 mM (E) 50 mM.

As shown in the figure, the strongest absorption spectra were performed by the sample of 1.5 mL Ag solution and 0.8 mL silver solution. These strong peaks represent to high number of the silver nanosheets and high area covered by the nanosheets.

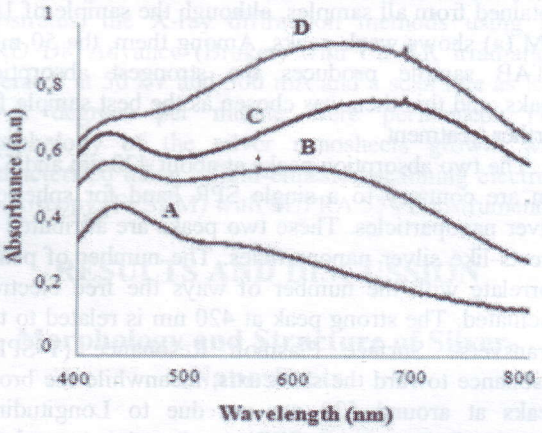

FIGURE 6. UV-Vis spectra of the silver-sheets at 0.8 mM PVP and 50 mM CTAB with volume of Ag solution of (A) 0.5 mL (B) 1.0 mL (C) 0.8 mL (D) 1.5 mL.

CONCLUSION

The current method of seed-mediated growth using a binary surfactant of CTAB and PVP has successfully grown a variety shapes of silver-nanosheets., including triangular, hexagonal, truncated-hexagonal, trapezium, circular and irregular-nanosheets. XRD pattern of the silver-nanosheets shows that the peaks (38.119° and 44.305°) are related to the diffractions from the (111) and (200) planes of fcc symmetry of silver nanosheets (JCPDS No. 01-087-0717), respectively.

The FESEM images of the silver-nanosheets grown on the ITO were clearly shown that almost all of the surface area of substrate (more than 85%) was covered by silver nanosheets in all samples. The edge-length size of the silver nanosheets/plates was observed to be in the range of 30 - 200 nm for the samples of 0.8 and 1.0 mL silver. The best concentration of binary surfactants that resulted highest density and strongest absorption spectra was of 0.8 mM PVP and 50 mM CTAB.

ACKNOWLEDGMENTS

We would like to thank DP2M, Ministry of Education and Culture, Republic Indonesia for financial support to this current research, with a Grant of Hibah Bersaing. We also thank Riau University and Institute of Microengineering and Nanoelectronics - Universiti Kebangsaan Malaysia for the use of laboratory facilities.

REFERENCES

1. J. J. Zhu, C. X. Kan and X. G. G. Zhu, *Journal of Materials Research* **22(6)**, 1479-1485 (2007).
2. F. R. Fan, DE. Y. Liu and Y. F. Wu, *Journal of the American Chemical Society* **130(22)**, 6949-6951 (2008).
3. J. Zhou, J. An and B. Tang, *Langmuir* **24(18)**, 10407-10413 (2008).
4. P. S. Mdluli and N. Revaprasadu, *Journal of Alloys and Compounds* **469**, 519-522 (2009).
5. M. Szymanska-Chargot, A. Gruszecka and A. Smolira, *Journal of Alloys and Compounds* **486**, 66-69 (2009).
6. C. M. Cobley, S. E. Skrabalak, D. J. Campbell and Y. Xia, *Plasmonics* **4(2)**, 171-179 (2009).
7. M. Liu, M. Leng, C. Yu, X. Wang and C. Wang, *Nano Res.* **3(12)**, 843-851 (2010).
8. S. Chen and D. L. Carroll, *Nano Letters* **2(9)**, 1003-1007 (2002).
9. S. Chen, Z. fan and D. L. Carroll, *Journal of Physical Chemistry B* **106(42)**, 10777-10781 (2002).
10. J. An, B. Tang and X. Ning, *Journal of Physical Chemistry C* **111(49)**, 18055-18059 (2007).
11. Iwantono, A. A. Umar, E. Taer and V. Asyana, *Journal of Materials Science Forum*. **756**, 112-118 (2013).
12. N. R. Jana, L. Gearheart and C. J. Murphy, *Chemical Communications* **7**, 617-618 (2001).
13. C. A. I. Xionghui and Z. Aixia, *Rare Metals* **29**, 407 (2010).
14. G. C. J. Swarnavalli, V. Joseph, V. Kannappan and D. Roopsingh, *Journal of Nanomaterials* **2011**, 1-5 (2011).